# On the Role of Shape in the Detection of Melanomas

Margarida Ruela
ISR, IST,
Lisbon, Portugal.

Catarina Barata
ISR, IST,
Lisbon, Portugal.

Teresa Mendonça
FCUP,
Porto, Portugal.

Jorge S. Marques
ISR, IST,
Lisbon, Portugal.

***Abstract*—This paper presents a study on the role of shape in the detection of melanomas in dermoscopy images. The contribution of shape-related features was assessed by developing a Computer-Aided Diagnosis (CAD) system whose classification is solely based on this type of features. Four shape descriptors were used, first separately and then simultaneously, to describe the images. Image segmentation was performed both manually, by an expert, and automatically, by using an Adaptive Thresholding algorithm. The best performances were $SE = 92\%$ and $SP = 74\%$, obtained for manually segmented images, and $SE = 92\%$ and $SP = 78\%$, obtained for automatically segmented images. These results were achieved by combining the shape descriptors and show that shape information plays an important role in melanoma detection. Furthermore, no degradation was observed when automatic segmentation methods are used, instead of manual ones.**

## I. Introduction

### A. Motivation

Melanomas are one of the most aggressive types of cancer. They result from an abnormal proliferation of melanocytic cells, which are responsible for the production of melanin, the dark pigment responsible for skin color. Due to these increased growth rates, the early detection of melanomas is crucial for the treatment of these lesions. In fact, if a melanoma is detected in the beginning of its development, chances are that it can be easily treated by a simple excision. However, if a melanoma has already metastasize, survival rate drops drastically and, in most cases, it is considered incurable. In a study performed in the United States, the five year relative survival, from 2002 to 2008, dropped from $98.2\%$ in the case of a localized melanoma to $15.1\%$ in the case of a metastasized melanoma [2].

Melanomas can usually be distinguished from other lesions due to their larger dimensions, variegation, asymmetric shape and/or due to the presence of differential structures [1]. Furthermore, they usually present a darker coloration. Fig. 1 shows (a) an example of a melanoma and (b) an example of a benign lesion. As one can observe, these lesions are easily differentiated by the above mentioned features.

Nevertheless, not all benign lesions are so easily differentiated from melanomas. Fig. 2 shows (a) another melanoma and (b) another a benign lesion, but now exhibiting similar features. Though they have different diagnosis, these lesions look quite similar. Therefore, due to possible similarity between melanomas and other lesions, naked eye diagnosis leads to unreliable results and jeopardizes the early detection of melanomas.

This work was supported by FCT in the scope of projects PTDC/SAUBEB/103471/2008 and PEst-OE/EEI/LA0009/2011.

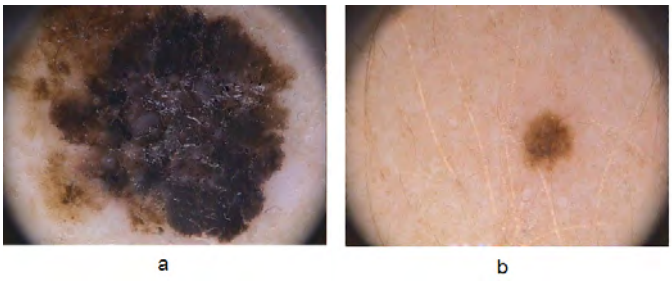


Fig. 1. Example of (a) a melanoma and (b) a benign lesion presenting different color and shape features.

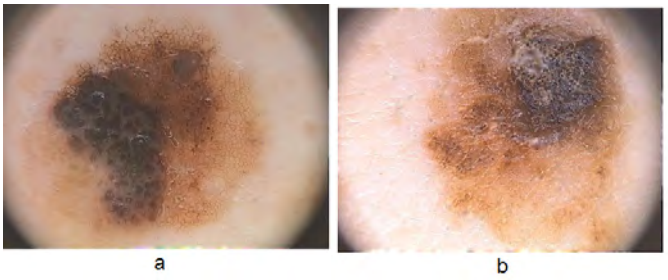


Fig. 2. Example of (a) a melanoma and (b) a benign lesion presenting similar color and shape features.

### B. State of the art

In order to differentiate benign from malign lesions, sophisticated diagnosis techniques are required. Dermoscopy is a good example of such a technique and has been used by dermatologists to diagnose pigmented skin lesions[1]. Dermoscopy images are acquired by using a dermatoscope which magnifies the lesions by a factor of 5-100 x, using special light and fluid. The acquisition process enhances the morphological structures present in the images and allows the visualization of structures not visible by naked eye [1]. Diagnostic methods such as the ABCD rule of dermoscopy [3] and the 7-point checklist [4] help dermatologists to make a more objective interpretation of the images.

However, the interpretation of the images may still be subjective and time consuming. Computer-Aided Diagnosis

(CAD) systems, which have been developed for the last two decades, intend to aid dermatologists in the classification task. CAD systems are usually divided into three main stages: image segmentation [5], [6], feature extraction and lesion classification [7], [8], [9], [10], [11].

Most CAD systems proposed in the literature combine several types of features extracted from the image, e.g., texture, color, shape and symmetry features [7], [8], [9], [14]. Regarding shape, simple features such as the area, perimeter, major and minor axis length, compactness index [8], [11], [12], rectangularity [7], [8], [9], ellipsoidality [14], eccentricity [8] and bulkiness [13], among others, have been used to describe the lesions. In addition to these features, some systems consider other features such as the symmetry about the minimum inertia axis [8], [11], [12], the fractal dimension [11], [13] and the irregularity index [15].

Shape features are never considered in isolation. They have always been considered together with other types of features and therefore it is not known how important is shape information in the automated detection of melanomas.

In this work we focus on shape. We wish to determine the contribution of shape to the classification of melanomas, we also intend to evaluate the performance of several shape descriptors and to determine the best combination of shape-related features.

## II. System Overview

The system developed in this work can be divided into three main stages: image segmentation, feature extraction and lesion classification. Fig. 3 shows an overall description of the proposed system. The system works as follows. Firstly, the system receives a dermoscopy image, $I$, which is submitted to the image segmentation block. This block computes a binary segmentation mask, $B$, whose active pixels define the lesion, see Fig. 4. Segmentation was performed both manually by an experienced dermatologist and automatically by using Adaptive Thresholding [5]. Examples of the segmentation contours generated by both methods are represented in Figs. 5, 8 and 9. We chose to use these two different segmentation strategies in order to assess the impact of different segmentation methods on the performance of the system.

Secondly, the segmentation mask generated in the first block proceeds to the feature extraction stage. As this study aims to assess the role of shape in the diagnosis of skin lesions, only shape-related features were extracted from the images. Furthermore, all the features were extracted from the binary image $B$, neglecting important information (e.g., lesion color and texture). The extracted features can be divided into four groups: simple shape features, symmetry-related features, moment invariants and Fourier descriptors.

In the last stage, the feature vector, $\mathbf{x}$, generated in the second block is submitted to a classifier, which returns the decision of the system, $y$. In this work, we opted to use the AdaBoost classifier. AdaBoost is used with a Decision Stump (DS) as weak classifier [16].

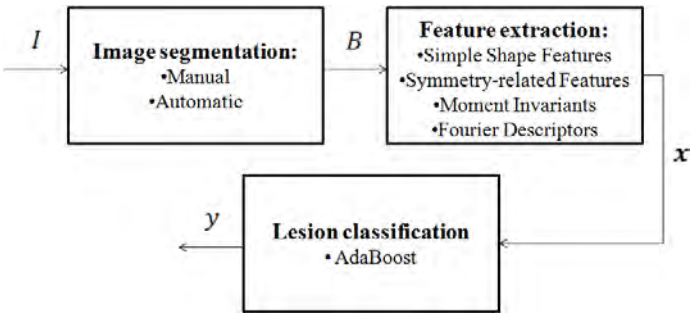


Fig. 3. Overall description of the system.

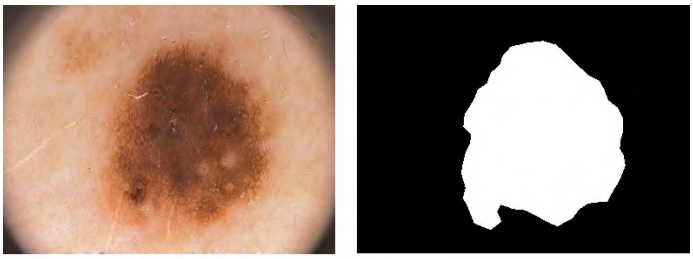


Fig. 4. Example of a (a) Dermoscopy image and (b) its correspondent binary mask. The white area of the mask corresponds to the skin lesion, whereas the black one represents the healthy tissue.

## III. Shape Features

As aforementioned, the shape features used in this work are organized in four groups: simple shape (SS) features, symmetry-related (SR) features, moment invariants (MI) and Fourier descriptors (FD). All these features were extracted solely from the binary segmentation masks.

### A. Simple Shape Features

In this work, we consider to be simple shape (SS) features the most simple shape-related features which can be extracted from the images as well as some features which can be derived from them. This group includes the lesion's area (A) in pixels, compactness, major and minor axis length and rectangularity. The compactness ($C = \frac{4\pi A}{P^2}$) corresponds to the ratio between the area of the lesion and the area of a circle with the same perimeter (P) as the lesion. The lengths of the major and minor axis are the maximum and minimum diameters of the lesion (in pixels) and the rectangularity of the lesion corresponds to the ratio between the area of the lesion and the area of the smallest rectangle able to contain the whole lesion [8], [12].

### B. Symmetry-related Features

In this work, the symmetry of the lesion is measured by using two different methods: i) the symmetry with respect to the principal axis and ii) the symmetry between opposite slices of the lesion. In both cases, the principal axes were determined by performing a Principal Component Analysis.

The symmetry about an axis is determined by overlapping one of the sides of the axis and the mirrored image of the other side. This measure of symmetry is computed by dividing

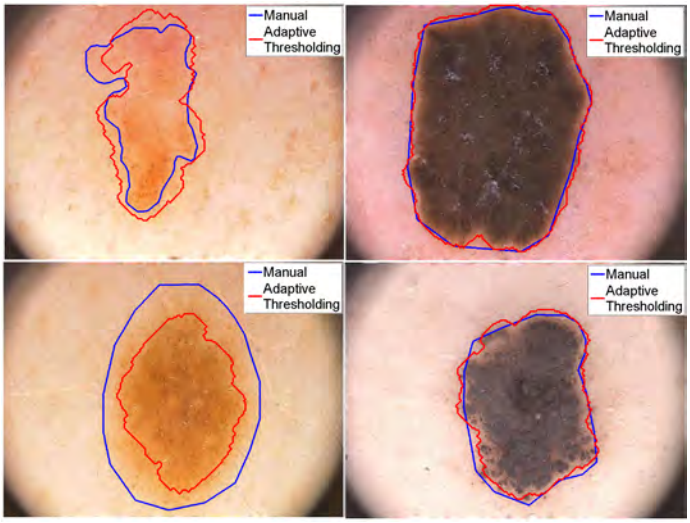


Fig. 5. Examples of segmentation contours obtained by manual segmentation (blue line) and by using the Adaptive Thresholding algorithm (red line).

twice the number of overlapping pixels by the total area of the lesion(in pixels). The symmetry of opposite slices is measured by dividing the image into an even number of slices with a common vertex: the lesion centroid. All the slices are defined by the intersection of the lesion with circular sectors with the same angle. The symmetry between two opposite slices is determined by overlapping the mirrored image of a slice with its opposite slice. The feature representing the symmetry between two slices is computed by dividing twice the number of overlapping pixels by the sum of the areas of the two slices (in pixels).

### C. Moment Invariants

Moment invariants are classic shape features proposed by Hu. Seven central moments of the object of interest are computed from the binary image and modified, in order to make them invariant to translation, rotation and scaling (see [17] for details).

### D. Fourier Descriptors

The Fourier Descriptors (FD) also provide shape information invariant to translation, rotation and scaling of the object of interest. They correspond to the coefficients, $c_k$, of the Discrete Fourier Transform of a *shape signature* [18], which is a 1D function that represents the shape of the object contained in the image. The shape signature used in this work is defined as follows

$$z(n) = x(n) + iy(n) \qquad n = 0, 1, ..., N-1, \quad (1)$$

where $i$ is the imaginary unit, $i^2 = -1$, $N$ is the number points selected from the boundary of the object and $(x(n), y(n))$ are the coordinates of the $n^{th}$ point. The selected points are equally spaced and separated by $\frac{1}{N}$ of the lesion perimeter. Since the sequence $z(n)$ is periodic with period $N$, it can be represented by a Fourier series and expressed as a function of complex Fourier coefficients $c_k, k \in \mathcal{Z}$.

However these coefficients are not invariant yet. Translation, rotation and scaling invariance is achieved after performing the following operations

$$d_k = \frac{|c_k|}{|c_1| + |c_2|} \qquad k = 1, 2, ..., N-1, \quad (2)$$

note that the first coefficient ($c_0$) is not considered.

## IV. Experimental Results and Discussion

### A. Database

The data-set used in this work contains images from the database PH$^2$ [20], collected in Hospital Pedro Hispano, in Matosinhos. This data-set comprises 167 lesions, from which 24 are melanomas ($\approx 14\%$). All the lesions whose boundary is not contained inside the image were discarded. The dermoscopy images were acquired during routine clinical examinations using a dermatoscope with $20\times$ magnification and were stored in JPEG format. Lesion diagnosis was performed by an experienced dermatologist and was, in some cases, confirmed by histological examination.

The preprocessement of the images consisted in hair and reflection removal by using directional filters in the former and a thresholding algorithm in the latter. Afterwards, an inpaintig algorithm was used to fill the resulting gaps [21].

### B. Evaluation Metrics

For each configuration of the system parameters, training and test were performed through Leave-One-Out Cross Validation (LOOCV). Performance was measured in terms of sensitivity (SE) and specificity (SP). The best performance was determined with the aid of a cost function that combines SE and SP. The adopted cost function is given by

$$C_T = 1 - \frac{3}{5}SE - \frac{2}{5}SP, \quad (3)$$

where SE has a greater weight because the misclassification of a melanoma has more severe consequences than the misdiagnosis of a non-melanoma lesion.

### C. Experimental Results and Discussion

The system developed in this work was tested using both manual and automatic segmentation methods. For each type of segmentation we assessed the performance of the system by using four shape descriptors (SS, SR, MI, FD). These descriptors were firstly tested individually and were posteriorly combined. Both SR and FD were defined by more than one configuration. In the former we varied the number of points sampled from the boundary of the lesions ($N \in \{16, 32, 64\}$). In the latter we used the two axis of symmetry ($A = 2$) and varied the number of slices ($S \in \{4, 8, 16\}$). Classification was performed using AdaBoost [16] with a Decision Stump (DS) as weak classifier. DS is a simple classifier, with few parameters to tune, which selects a single feature. In this stage we tried to optimize the weight ($\alpha$) given to melanoma patterns ($\alpha \in \{1, 2\}$) and the number ($T$) of weak classifiers ($T \in \{2, 3, ..., 20\}$), see [16] for more details. A total of 684 system configurations were trained and evaluated by LOOCV.

| Descriptor | Manual Segmentation | | | | | | | | Automatic Segmentation | | | | | | | |
|---|---|---|---|---|---|---|---|---|---|---|---|---|---|---|---|---|
| | SE | SP | Cost | $\alpha$ | T | A | S | N | SE | SP | Cost | $\alpha$ | T | A | S | N |
| SS | 88 | 67 | 0.204 | 2 | 2-5 | - | - | - | 92 | 69 | 0.172 | 1 | 2 | - | - | - |
| SR | 88 | 48 | 0.280 | 2 | 4 | 2 | 16 | - | 79 | 59 | 0.290 | 2 | 4 | 2 | 16 | - |
| MI | 88 | 54 | 0.256 | 2 | 16 | - | - | - | 79 | 57 | 0.298 | 1 | 5 | - | - | - |
| FD | 75 | 49 | 0.354 | 2 | 3 | - | - | 64 | 71 | 79 | 0.258 | 1 | 3,4 | - | - | 16 |
| SS+MI | 88 | 71 | 0.188 | 2 | 19 | - | - | - | **92** | **78** | **0.136** | **2** | **4** | - | - | - |
| SS+SR+MI | **92** | **74** | **0.152** | **2** | **4** | **2** | **4** | - | 88 | 83 | 0.140 | 1 | 6 | 2 | 4 | - |
| All | 88 | 75 | 0.172 | 2 | 4 | 2 | 4 | 16 | 88 | 80 | 0.152 | 1 | 2 | 2 | 4 | 16,64 |

TABLE I

BEST PERFORMANCE OF THE SYSTEM FOR EACH OF THE SEGMENTATION METHODS AND FOR EACH DESCRIPTOR. THE PARAMETERS FILLED WITH '-' INDICATE THAT THE PARAMETER IS NOT APPLIED TO THAT DESCRIPTOR.

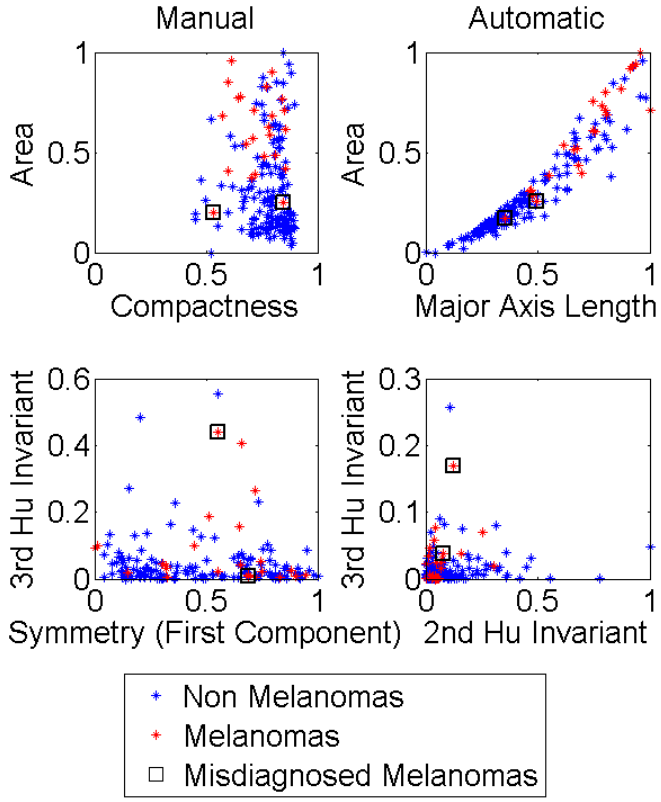


Fig. 6. Scatter plots of the four most selected features selected by AdaBoost for manual segmentation (area, compactness, symmetry and $3^{rd}$ Hu invariant) and automatic segmentation (area, major axis length and $2^{nd}$ and $3^{rd}$ Hu invariants). Non-melanomas are represented in blue, melanomas are represented in red. Both area and major axis length were normalized by using MAXMIN normalization.

Table I shows the best results achieved by each shape descriptor and by each segmentation method. As presented in the table, regardless of the segmentation method, SS was by far the individual descriptor which led to the best performance (minimum cost). For example, the manually segmented images achieved a performance of $SE = 88\%$ and $SP = 67\%$ by using this descriptor. This result was achieved by using $\alpha = 2$ and four different values of $T$, $T \in \{2, 3, 4, 5\}$. The features which were more frequently selected by the weak classifiers were the area, the compactness and the length of the major axis.

The performance achieved by using the automatically segmented images was slightly better with $SE = 92\%$ and $SP = 69\%$. This result was obtained by using $\alpha = 1$ and $T = 2$. In this case, the area of the lesion and the length of the minor axis were the most selected features.

A best performance from the system using automatic segmentation is a rather unexpected result. However, by analyzing the segmentation masks generated by both methods, one observes that the automatic segmentation requires relatively sharp color transitions in order to identify the border of the lesion. Therefore, the lighter regions from the border of the lesion are sometimes neglected by the segmentation algorithm. However, these regions usually provide valuable information and are considered by dermatologists when performing manual segmentation, see Fig. 5. As a result, manual segmentation will most times originate larger lesion areas. Since the SS features are strongly correlated to the size of the lesion and since non-melanomas usually have smaller dimensions, the larger areas generated by manual segmentation may lead to the misdiagnosis of non-melanomas. Melanomas do not face this problem as often as non-melanomas because they usually present darker colors which facilitates the detection of the lesion's border. However, in a few cases, some of the lighter regions of melanomas that present high color variation may be neglected by the automatic segmentation algorithms generating even more asymmetric shapes, which when solely using shape descriptors may benefit this segmentation technique.

The best performance of the system, $SE = 92\%$ and $SP = 78\%$, was achieved by using automatic segmentation and resulted from the combination of two descriptors: SS and MI. This result was achieved by using $\alpha = 2$ and $T = 4$. The most selected features, by the weak classifiers, were the area, the major axis length and the second and third Hu invariants. The combination of these descriptors with SR or both SR and FD leads to an increase of SP, but to a decrease in SE and an increase in cost and, thus, the performance of the system does not improve. An almost as good performance, $SE = 92\%$ and $SP = 74\%$, was achieved by using the manual segmentation and resulted from the combination of three descriptors: SS, SR and MI. This result was achieved by using $\alpha = 2$ and $T = 4$. The most selected features were the area, the length of the major axis, the symmetry about the first principal component and the third Hu invariant. The combination of all four sets of descriptors does not improve the performance.

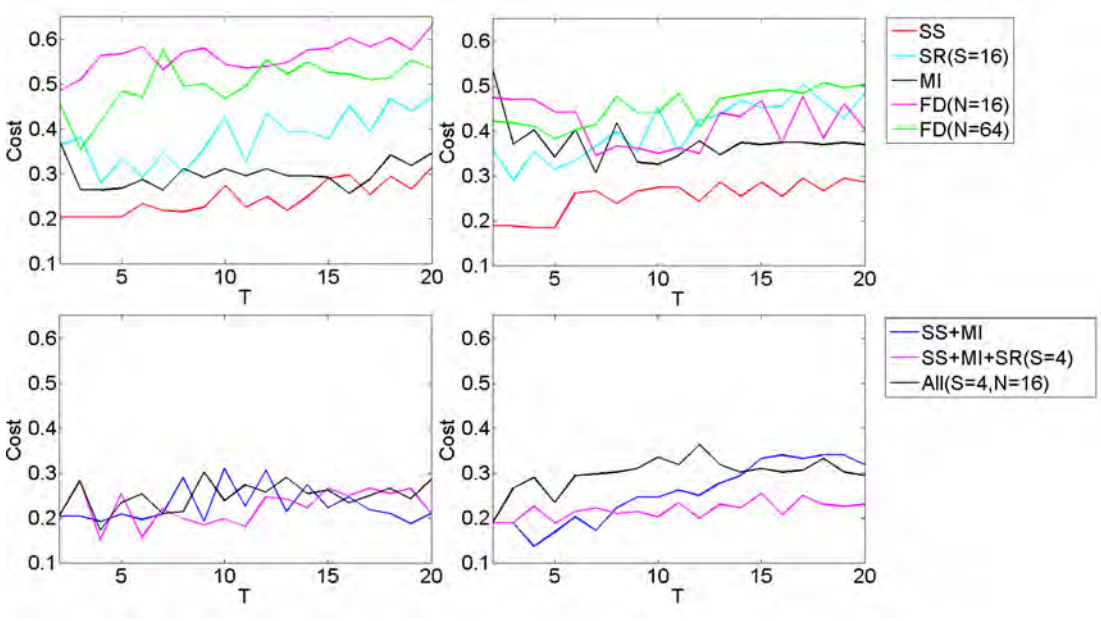


Fig. 7. System performance (cost) as a function of the number of weak classifiers (T) ($\alpha = 2$) for the individual descriptors (top row) and for the combined descriptors (bottom row). On the left column are represented the results obtained by using manual segmentation whereas on the right column are represented the results obtained by using automatic segmentation.

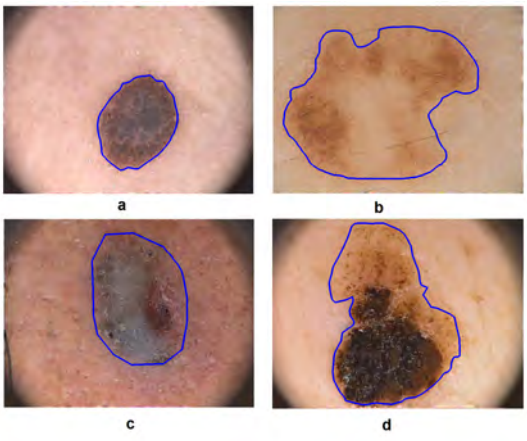


Fig. 8. Examples of images classified by the best configuration of the system using manual segmentation: (a) TN, (b) FP, (c) FN and (d) TP. The blue line represents the manual segmentation.

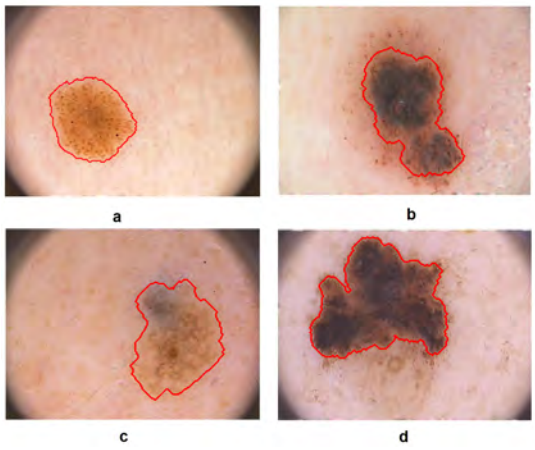


Fig. 9. Examples of images classified by the best configuration of the system using automatic segmentation: (a) TN, (b) FP, (c) FN and (d) TP. The red line represents the automatic segmentation.

Fig. 6 shows scatter plots of the four most selected features by using the best configuration of the system for both manual and automatic segmentation masks. Fig. 6 shows that this is a difficult problem, because there is a big overlap between the features of both classes. However, in both cases it is possible to see that the misdiagnosed melanomas were the ones which presented the smallest lesion area. Nevertheless, given the difficulty of the problem, the results presented in Table I are quite surprising.

Since the best results were achieved using $\alpha = 2$, let us analyze how the performances vary with $T$, see Fig. 7. On the top row we compare the performance of each shape descriptor type, for both segmentation methods, whereas on the bottom row we compare the performance of the combined descriptors.

Figs. 8 and 9 show, for the best configuration of the system for each segmentation technique (manual and by using the Adaptive Thresholding algorithm), examples of true positives (TP), false positives (FP), true negatives (TN) and false negatives (FN). TP and TN are, respectively, melanomas and non-melanomas which were correctly classified whereas FN and FP are, respectively, misclassified melanomas and non-melanomas.

## V. Conclusions and Future Work

This paper presents a study on the role of shape-related features in the detection of melanomas using dermoscopy images. This role was assessed by developing a CAD system in which classification is solely based on shape descriptors. Four sets of shape descriptors (SS, SR, MI and FD) were separately and jointly analyzed. Furthermore, the system was tested using both manually and automatically segmented images. The descriptors which achieved the best individual performance were simple shape (SS) features, regardless the applied segmentation method. The best performance, $SE = 92\%$ and $SP = 78\%$, was achieved by using the automatically segmented images and the combination of SS and moment invariants (MI) descriptors. The results obtained with manually segmented images are similar, $SE = 92\%$ and $SP = 74\%$, and were achieved by using a combination of SS, symmetry-related (SR) and MI descriptors. According to these results, we conclude that shape-related features have an important role in the detection of melanomas. In addition, we may also conclude that classification by using shape descriptors is fairly robust to a change in the segmentation method.

In a previous studies such as [10], [22], the role of color and texture descriptors were evaluated by also using subsets of the $PH^2$ database [20]. In [22], it is performed a study on the role of color features in the detection of melanomas. The best configuration of the system achieved a performance of SE=100% and SP=93%, using a subset of the dataset used in this paper comprising 14 of the melanomas and 134 of the non melanomas. In [23] color and texture features are studied individually and combined. The combination of these features lead to a performance of SE=96% and SP=82%. This result was obtained by using a dataset with 151 non-melanomas and 25 melanomas, most of which are also used in this paper.

Since color and texture descriptors were able to achieve slightly better results, in the future, it would be interesting to enrich these shape descriptors with the best set of texture and color features, determined in previous studies. Furthermore, it would also be interesting to analyze the behavior of these shape descriptors when applied to larger databases.

## VI. Acknowledgments

The authors would like to thank Dr. J. Rozeira from Hospital Pedro Hispano for kindly providing the dermoscopy images used in this work. Most of these images belong to $PH^2$ database which will soon be freely available [20].

## References

[1] Dermoscopy. http://www.dermoscopy.org/

[2] Howlader N, Noone AM, Krapcho M, Neyman N, Aminou R, Altekruse SF, Kosary CL, Ruhl J, Tatalovich Z, Cho H, Mariotto A, Eisner MP, Lewis DR, Chen HS, Feuer EJ, Cronin KA SEER Cancer Statistics Review, 1975-2009 (Vintage 2009 Populations) National Cancer Institute Bethesda, MD.

[3] Nachbar, F., Stolz, W., Merkle, T., Cognetta, A. B., Vogt, T., Landthaler, M., Bilek, P., Braun-Falco, O., Plewig, G.: The ABCD rule of dermatoscopy. High prospective value in the diagnosis of doubtful melanocytic skin lesions. J Am Acad Dermatol 30(4), 551–559 (1994)

[4] Argenziano, G., Fabbrocini, G., Carli, P., De Giorgi, V., Sammarco, E., Delfino, M.: Epiluminescence microscopy for the diagnosis of doubtful melanocytic skin lesions. Comparison of the ABCD rule of dermatoscopy and a new 7-point checklist based on pattern analysis. Arch Dermatol 134, 1563–1570 (1998).

[5] Barata, C., Ruela, M., Francisco, M., Mendonça, T. and Marques, J. S., Two Systems for the Detection of Melanomas in Dermoscopy Images using Texture and Color Features, IEEE System Journal, accepted, 2013.

[6] Celebi, M E., Wen, Q., Hwang, S., Iyatomi, H., Schaefer, G.: Lesion Border Detection in Dermoscopy Images Using Ensembles of Thresholding Methods. Skin Research and Technology 19, 252–258 (2013).

[7] Iyatomi, H., Celebi, M. E., Oka, H., Tanaka, M.: An Improved Internet-Based Melanoma Screening System with Dermatologist-like Tumor Area Extraction Algorithm. Comp Medical Imaging and Graphics 32, 566–579 (2008).

[8] Celebi, M. E., Kingravi, H. A., Uddin, B.,Iyatomi, H., Aslandogan, Y. A., Stoecker, W. V., Moss, R. H.: A methodological approach to the classification of dermoscopy images. Comp Medical Imaging and Graphics 31(6), 362–371 (2007).

[9] Ganster, H., Pinz, A., Rohrer, R., Wildling, E., Blinder, M., Kittler H.: Automated Melanoma Recognition. IEEE Trans on Biom Eng 20(3), 233–239 (2001).

[10] Marques, J.S., Barata, C., Mendonça, T.: On the role of texture and color in the classification of dermoscopy images. Engineering in Medicine and Biology Society (EMBC), 2012 Annual International Conference of the IEEE.

[11] Andreassi, L., Perotti, R., Rubegni, P., Burroni, M., Cevenini, G., Biagioli, M., Taddeucci, P., Dell'Eva, G., Barbini, P.: Digital Dermoscopy Analysis for the Differentiation of Atypical Nevi and Early Melanoma: a new quantitative semiology. Archives of Dermatological Research 135, 1459–1465 (1999).

[12] Ecral, F., Chawla, A., Stoecker, W. V., Lee, H.-C., Moss, R. H.: Neural network diagnosis of malignant melanoma from color images. IEEE Trans on Biom Eng 41(9), 837–845 (1994).

[13] Claridge, E., Hall, P. N., Keefe, M., Allen, J.P.: Shape analysis for classification of malignant melanoma. J. Biomed. Eng. 14, 229-234 (1992).

[14] Rubegni, P., Cevenini, G., Burroni, M., Perotti, R., Dell'Eva, G., Sbano, P., Miracco, C., Luzi, P., Tosi, P., Barbini, P., Andreassi, L.: Automated diagnosis of pigmented skin lesions. Inter J. of Cancer 101, 575–580 (2002).

[15] Lee, T. K., McLean, D. I., Atkins, M. S.: Irregularity index: A new border irregularity measure for cutaneous melanocytic lesions. Medical Image Analysis 7, 47–64 (2003).

[16] Viola, P., Michael, J.: Robust real-time face detection. Inter J of Comp Vision 57, 137–154 (2004).

[17] Hu, M.-K.: Visual Pattern Recognition by Moment Invariants. IRE Transactions on Information Theory 49, 179–187 (1962).

[18] Zhang, D., Lu, G.: A Comparative Study on Shape Retrieval Using Fourier Descriptors with Different Shape Signatures. Journal of Visual Communication and Image Representation 14(1), 41–60 (2003).

[19] Jain, Anil K.: Fundamentals of digital image processing. Prentice-Hall, Inc. (1989).

[20] Mendonça, T., Ferreira, P. M., Marques, J., Marçal, A. R. S., Rozeira, J.: Accepted for presentation in Proc. $PH^2$ - A Dermoscopic Image Database for Research and Benchmarking. IEEE EMBC, 2013.

[21] Barata, C., Marques, J. S., Rozeira, J.: A System for the Detection of Pigment Network in Dermoscopy Images Using Directional Filters. IEEE Trans on Biom Eng 59(10), 2744–2754(2012)

[22] Ruela, M.,Barata, C., Mendonça, T.,Marques, J.S.: What is the role of color in dermoscopy analysis?. Accepted for presentation in Proc. of IbPRIA 2013 - 6th Iberian Conference on Pattern Recognition and Image Analysis, Madeira, Portugal, 2013.

[23] Barata, C., Ruela, M., Marques, J S. and Mendonça, T.: A Bag-of-Features Approach for the Classification of Melanomas in Dermoscopy Images: The Role of Color and Texture Descriptors. Accepted for publication in Computer Vision Techniques for the Diagnosis of Skin Cancer 2013.